OPEN ACCESS



Composition of Giants 1° North of the Galactic Center: Detailed Abundance Trends for 21 Elements Observed with IGRINS

Govind Nandakumar¹, Nils Ryde¹, Gregory Mace², Kyle F. Kaplan², Niels Nieuwmunster^{1,3}, Daniel Jaffe², R. Michael Rich⁴, Mathias Schultheis³, Oscar Agertz¹, Eric Andersson⁵, Christopher Sneden², Emily Strickland⁶, and Brian Thorsbro³

Division of Astrophysics, Department of Physics, Lund University, Box 43, SE-22100 Lund, Sweden; govind.nandakumar@astro.lu.se
 Department of Astronomy and McDonald Observatory, The University of Texas, Austin, TX 78712, USA
 Observatoire de la Côte d'Azur, CNRS UMR 7293, BP4229, Laboratoire Lagrange, F-06304 Nice Cedex 4, France
 Department of Physics and Astronomy, UCLA, 430 Portola Plaza, Box 951547, Los Angeles, CA 90095-1547, USA
 Department of Astrophysics, American Museum of Natural History, 200 Central Park West, New York, NY 10024, USA
 Department of Physics and Astronomy, The University of Utah, Salt Lake City, UT 84112, USA
 Received 2023 December 7; revised 2024 January 11; accepted 2024 January 24; published 2024 March 20

Abstract

We report the first high-resolution, detailed abundances of 21 elements for giants in the Galactic bulge/bar within 1° of the Galactic plane, where high extinction has rendered such studies challenging. Our high-signal-to-noise-ratio and high-resolution, near-infrared spectra of seven M giants in the inner bulge, located at $(l,b) = (0^{\circ}, +1^{\circ})$, are observed using the IGRINS spectrograph. We report the first multichemical study of the inner Galactic bulge by investigating, relative to a robust new solar neighborhood sample, the abundance trends of 21 elements, including the relatively difficult to study heavy elements. The elements studied are: F, Mg, Si, S, Ca, Na, Al, K, Sc, Ti, V, Cr, Mn, Co, Ni, Cu, Zn, Y, Ce, Nd, and Yb. We investigate bulge membership of all seven stars using distances and orbital simulations, and we find that the most metal-poor star may be a halo interloper. Our investigation also shows that the inner bulge as close as 1° north of the Galactic Center displays a similarity to the inner disk sequence, following the high- $[\alpha/Fe]$ envelope of the solar vicinity metal-rich population, though no firm conclusions for a different enrichment history are evident from this sample. We find a small fraction of metal-poor stars ([Fe/H] > -0.5), but most of our stars are mainly of supersolar metallicity. Fluorine is found to be enhanced at high metallicity compared to the solar neighborhood, but confirmation with a larger sample is required. We will apply this approach to explore the populations of the nuclear stellar disk and the nuclear star cluster.

Unified Astronomy Thesaurus concepts: Galactic bulge (2041); Chemical abundances (224); Galactic archaeology (2178); Solar neighborhood (1509); M giant stars (983); Near infrared astronomy (1093); High resolution spectroscopy (2096)

1. Introduction

Our canonical view of the chemical evolution of the Galactic bulge is grounded in a stellar population of age >10 Gyr that formed early and rapidly. McWilliam & Rich (1994) found the bulge enhanced in α elements relative to the thick disk, while Matteucci & Brocato (1990) illustrated the expected elevated trend of $[\alpha/\text{Fe}]$ versus [Fe/H]. Subsequent modeling of the chemical evolution of the bulge adds detail (e.g., Matteucci et al. 2019) and posits a multiphase evolution of the bulge, with the possibility of a disk-like population forming, following a pause in star formation after the early starburst that gives rise to the bulge. The picture of α -enhancement relative to the thin disk has largely held firm (e.g., Zoccali et al. 2006; Fulbright et al. 2007; Meléndez et al. 2008; Ryde et al. 2010; Hill et al. 2011; Johnson et al. 2014; Bensby et al. 2017; Jönsson et al. 2017; Lomaeva et al. 2019; Nieuwmunster et al. 2023) and a picture is emerging of the bulge appearing to be similar to the thick disk, but extended to higher metallicity. This was also suggested by Di Matteo (2016), where the thick-disk (high- α) and the metal-poor thin-disk (low- α , [Fe/H] $\lesssim -0.3$) stellar populations in the solar neighborhood are referred to as the

Original content from this work may be used under the terms of the Creative Commons Attribution 4.0 licence. Any further distribution of this work must maintain attribution to the author(s) and the title of the work, journal citation and DOI.

"inner disk sequence" and the "outer disk sequence," respectively. Further, the metal-rich thin-disk population that is joined by the "inner disk sequence" is referred to as the "inner thin disk," and it is considered to be the same structure as the thick-disk or "inner disk sequence" (see also Haywood et al. 2013). Based on this, the metal-rich component (A) and metal-poor components (B, C) in the bulge from Ness et al. (2013) are associated with the "inner thin disk" and "inner disk sequence," respectively. A similar scenario is borne out in the cosmological zoom simulation VINTERGATAN (Agertz et al. 2021; Renaud et al. 2021) of a Milky Way-like galaxy, where the solar neighborhood chemical thin-disk stars formed in an outer disk.

Industrial-scale spectroscopy of the bulge and disk by the APOGEE project (e.g., Hayden et al. 2015; Queiroz et al. 2020, 2021) finds a bifurcated trend in $[\alpha/\text{Fe}]$ versus [Fe/H] as a function of radius in the Galaxy, with the inner $2\,\text{kpc}$ dominated by a high- α population and a disk-like, low- α population more or less disconnected, in contrast to the continuous trends in $[\alpha/\text{Fe}]$ versus [Fe/H] found earlier. Meanwhile, Zasowski et al. (2019) found the lack of bimodality in the $[\alpha/\text{Fe}]$ distributions at subsolar metallicity to suggest that the abundances are dominated by a single chemical evolutionary sequence using ${\sim}4000\,\text{K/M}$ giants in APOGEE Data Release (DR) 14/DR15 that are at galactocentric distances $R\leqslant 4.0\,\text{kpc}$.

 Table 1

 Observational Details of the Seven M Giants

Star	R.A.	Decl.	Date (UT)	$J_{ m 2MASS} \ m (mag)$	H _{2MASS} (mag)	K _{2MASS} (mag)	S/N_H S/N_K (per resolution element)	
BP1_1	17:41:49.98	-28:27:32.70	2016-05-23	12.02	10.57	9.99	50	70
BP1_2	17:41:56.10	-28:23:36.68	2016-05-24	12.28	10.73	10.02	50	50
BP1_3	17:41:44.96	-28:28:06.37	2016-05-28	11.42	10.12	9.67	80	90
BP1_5	17:41:56.59	-28:25:37.60	2016-06-18	11.69	10.24	9.70	60	60
BP1_6	17:41:27.03	-28:22:49.23	2016-06-19 and 2016-07-05	11.62	10.13	9.54	130	110
BP1_7	17:41:38.81	-28:28:39.89	2016-06-20	11.74	10.49	9.52	90	70
BP1_9	17:41:36.94	-28:23:41.07	2016-07-06	11.96	10.38	9.72	90	80

We stand on the threshold of the vastly larger production of industrial-scale spectroscopy by the MOONS project and Sloan Digital Sky Survey V. The former, like APOGEE, will employ the infrared H band to report compositions for \sim 15 elements at $R\sim$ 20,000 and do so, ultimately, for millions of stars.

As studies of the bulge/bar/inner galaxy increase, it has become appreciated that its star formation history may be more complex (Bensby et al. 2017), and even reassessments of age (Joyce et al. 2023) support an age range among the most metalrich stars. Johnson et al. (2022) find a striking concentration of bulge/bar metal-rich stars in the Galactic plane. Unfortunately, the precision and breadth of spectroscopy has failed to keep pace with these advances.

The inner bulge regions, i.e., regions within $|b| < 2^{\circ}$, host the Milky Way nuclear stellar disk (NSD) and nuclear star cluster (NSC), which are also ubiquitous in other galaxies (Neumayer et al. 2020). But detailed investigations into the chemistry of different stellar populations in the inner bulge regions have been limited to a handful of spectroscopic observations with only limited numbers of stars analyzed in these regions (for details, see the introduction and references in Nandakumar et al. 2018). This is due to the crowding and dust obscuration along the line of sight toward the inner bulge that demands observations at infrared wavelengths. Thus, more near-infrared spectroscopic observations are necessary to decipher the chemistry of the inner bulge regions.

Here we report on a small sample of bulge/bar candidate giants near the Galactic plane that are compared with an identically observed sample of solar neighborhood stars, using the Immersion GRating INfrared Spectrograph (IGRINS; Wang et al. 2010; Yuk et al. 2010; Gully-Santiago et al. 2012; Moon et al. 2012; Jeong et al. 2014; Park et al. 2014). The bulge/bar candidate giants are chosen from a field along the northern minor axis at $(l = 0^{\circ}, b = +1^{\circ})$, which is a region with relatively low extinction that is observable with the 2.7 m (107 inch) Harlan J. Smith Telescope at McDonald Observatory. IGRINS is able to record both the infrared H and K bands $(1.45-2.5 \,\mu\text{m})$ simultaneously at R = 45,000, double the resolution of the "APOGEE-like" surveys, and allows for the detailed analysis of a wealth of spectral lines, enabling detailed studies of stellar abundances for a range of different elements. Although the sample we report here is small, we have the advantage of a direct comparison with the solar neighborhood sample, and we can investigate the detailed abundances of 21 elements for these stars only 1° from the Galactic plane. As has already been hinted at by Nieuwmunster et al. (2023), differences between this population and the thick disk are subtle at best. The aim of this study—the careful, detailed analysis of our new sample compared to the Nandakumar et al. (2023a)

solar vicinity study—is to provide a well-established baseline for the study of the chemical evolution of this region, and to make clear the observational challenges as this work proceeds to larger samples. Finally, this work will stand in contrast to the future industrial-scale samples that will emerge in the coming years.

In this work, we will thus determine elemental abundances and their trends with metallicities for up to 21 elements for seven M giants located in the inner degree region of the Galactic Center along the northern minor axis $(l=0^{\circ})$ $b=+1^{\circ}$). These abundances are derived based on a consistent and systematic spectroscopic analysis of IGRINS spectra. The details of the observations and data reduction are provided in Section 2, followed by the details of the spectroscopic and dynamic analysis in Section 3. In Section 4, we show the elemental abundance trends for different groups of elements (α , odd-Z, iron-peak, and neutron-capture elements) and also compare with the trends for the same group of elements for the 50 solar neighborhood stars, observed and analyzed with the same setup. We discuss our results in the context of the Galactic bulge and inner Milky Way structures, and we compare with inner Milky Way abundance trends from APOGEE in Section 5. We make our final conclusions in Section 6.

2. Observations and Data Reduction

In order to investigate the chemical compositions and elemental trends of stars close to the Galactic plane, we have observed the entire H and K bands (1.5–1.75 and 2.05–2.3 μ m, respectively) of nine M giants with IGRINS at high spectral resolution, $R \sim 45,000$. The observations were carried out with the 2.7 m (107 inch) Harlan J. Smith Telescope at McDonald Observatory in 2016 May–July; see Table 1. However, only the seven stars that have high enough signal-to-noise ratios (S/Ns >50 per pixel) for a precise abundance analysis will be used in the following abundance analysis. We show the locations of these seven stars (the red circles) in the K versus J - K color magnitude diagram with and without extinction correction in the bottom and top panels of Figure 1, respectively. As a reference sample, we use the 50 M giants in the solar neighborhood analyzed in Nandakumar et al. (2023a, 2024) and Nandakumar et al. (2023b). These stars were observed with IGRINS in the same way as the inner bulge stars presented here.

The spectral reductions were done with the IGRINS PipeLine Package (Lee et al. 2017) to optimally extract the telluric-corrected, wavelength-calibrated spectra after flat-field correction (Han et al. 2012; Oh et al. 2014). The spectra were

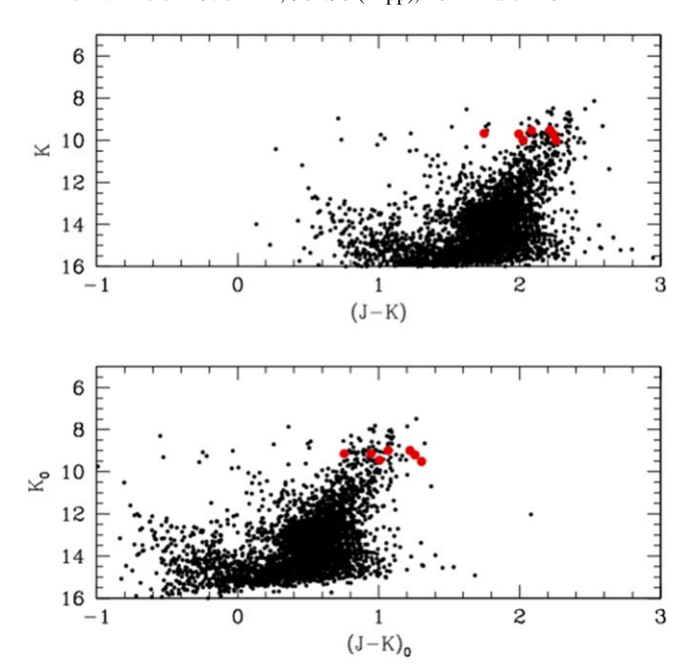


Figure 1. K vs. J-K color–magnitude diagram without extinction correction (top panel) and with extinction correction (bottom panel) for the stars in the $l=0^{\circ},\,b=+1^{\circ}$ field. The seven inner bulge giants observed and analyzed in this work are shown by the red circles.

then resampled and normalized in iraf (Tody 1993), but to take care of any residual modulations in the continuum levels, we put considerable focus on defining specific local continua around every line that elemental abundances were determined from. Finally, the spectra are shifted to laboratory wavelengths in air after a stellar radial velocity correction. The average S/Ns⁷ of the spectra of the giants close to the plane are in the range 60–130 (see Table 1).

3. Analysis

In order to minimize any systematic uncertainties, measurements of the stellar abundances need to be carried out differentially with respect to the stellar populations in the solar neighborhood. It is then imperative to observe stars of similar spectral types (here, M giants) both in the inner Milky Way and in the solar neighborhood regions, using the same instrument with the same wavelength range and spectral resolution. Furthermore, the same pipelines and techniques must be used in the determination of the stellar parameters and elemental abundances.

3.1. Spectroscopic Analysis

Nandakumar et al. (2024) determined abundances of the same 21 elements from the exact same lines for 50 close-by M giants (<4000 K) also from high-resolution spectra observed with IGRINS in the same mode. They demonstrated that M giants observed at high spectral resolution in the H and K bands (1.5–2.4 μ m) can yield both accurate and precise abundance ratio trends versus metallicity for all these elements. The 50 solar neighborhood stars will serve as the reference sample here.

Similar to Nandakumar et al. (2024), the spectroscopic analysis of the seven inner bulge M giants in this work has been carried out with the spectral synthesis method using the spectroscopy made easy (SME; Valenti & Piskunov 1996, 2012) tool in combination with the grid of onedimensional Model Atmospheres in a Radiative and Convective Scheme stellar atmosphere models (Gustafsson et al. 2008). We use the method provided by Nandakumar et al. (2023a) to determine the stellar parameters for the inner bulge stars. In this method, the effective temperature is mainly constrained by selected T_{eff} -sensitive OH lines, the metallicity by selected Fe lines, the microturbulence by different sets of weak and strong lines, and the C and N abundances by selected CO and CN molecular lines. The surface gravity is determined based on the effective temperature and metallicity by means of the Yonsei-Yale isochrones, assuming old ages of 2-10 Gyr (Demarque et al. 2004), which are appropriate for low-mass giants. This is the same method used to determine the stellar parameters for the reference sample of 50 solar neighborhood M giants. The method and its validation with nearby benchmark stars are described in detail in Nandakumar et al. (2023a). We note that there also exists an excellent method for determining the effective temperature through a line-depth method for IGRINS spectra, as presented in Afşar et al. (2023). We choose, however, to get all the stellar parameters through spectral synthesis.

The oxygen abundances for the inner bulge stars have been assumed to follow the enhanced values of the thick-disk population based on findings from previous studies (for example, see Rojas-Arriagada et al. 2017; Nieuwmunster et al. 2023). Hence, during the parameter determination of the seven inner bulge stars, we assumed oxygen abundances (corresponding to the metallicity of each star) from the thick-disk [O/Fe] versus [Fe/H] trend determined for solar neighborhood stars in Amarsi et al. (2019; see also the simple functional form of this trend in Figure 1 in Nandakumar et al. 2023a). The effective temperatures of the seven inner bulge stars lie in the range of 3500-4000 K and the surface gravities in the range of 0.6–1.7 dex. Two stars are metal-poor (BP1_5: $[Fe/H] \sim -1.14 \text{ dex}$; and $BP1_7$: $[Fe/H] \sim -0.65 \text{ dex}$), and the rest are all metal-rich or supersolar ($[Fe/H] \sim$ 0.03–0.23 dex). Our final stellar parameters and [C/Fe], [N/Fe], and [O/Fe] results, determined in this way, are listed in Table 2.

We will use the method outlined in Nandakumar et al. (2023a) and Nandakumar et al. (2024) to determine the elemental abundances for the 21 elements and Fe. The atomic lines used are given in these references and the abundances are calculated assuming non–local thermodynamic equilibrium (NLTE) for C, N, O, Na, Mg, Al, Si, K, Ca, and Fe (Lind et al. 2017; Amarsi et al. 2020 and 2016 with subsequent updates; A. M. Amarsi private communication), with the departure coefficients computed using the message passing interface-parallelized NLTE radiative transfer code Balder (Amarsi et al. 2018). The line data for the CO, CN, and OH lines were adopted from the line lists of Li et al. (2015), Brooke et al. (2016), and Sneden et al. (2014), respectively. The molecular lines are important, since they blend with and affect the measurement of atomic spectral lines.

⁷ The S/Ns are provided by the Raw & Reduced IGRINS Spectral Archive (Sawczynec et al. 2022) and each is the average S/N for *K* band and is per resolution element. It varies over the orders and it is lowest at the ends of the orders.

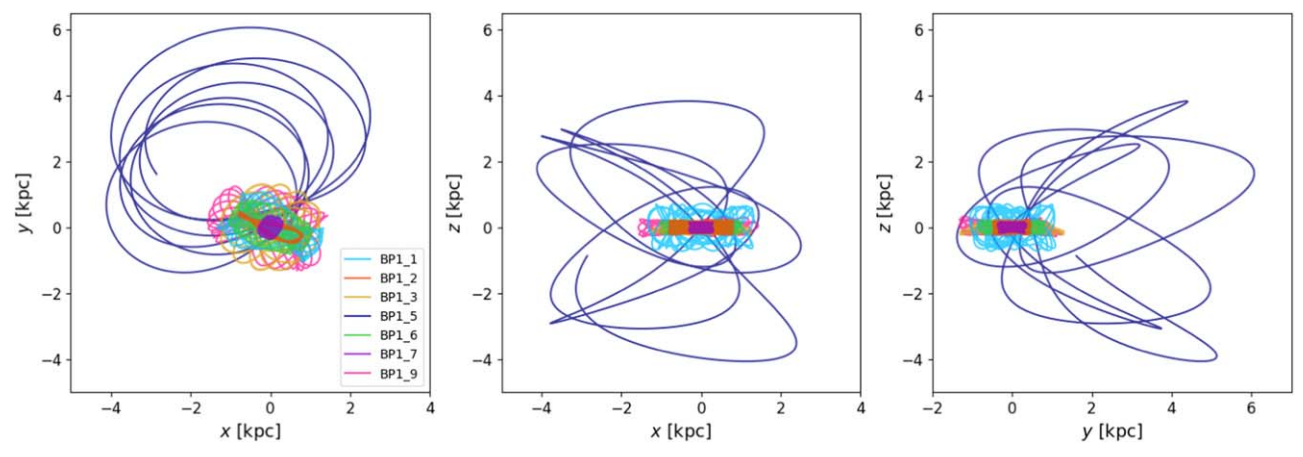


Figure 2. Orbits of the seven M giants of the $(l, b) = (0^{\circ}, +1^{\circ})$ field in (x, y) (left panel), (x, z) (middle panel), and (y, z) (right panel).

 Table 2

 Stellar Parameters, Galactocentric Radial Velocities, and Bulge Membership of the Seven M Giants

Star	T _{eff} (K)	$\log g \log(\text{cm s}^{-2})$	[Fe/H] (dex)	ξ_{micro} (km s^{-1})	[C/Fe] (dex)	[N/Fe] (dex)	[O/Fe] (dex)	V_R (km s ⁻¹)	Population
BP1_1	3491	0.79	0.21	1.72	0.11	0.05	0.04	41.14	Inner bulge
BP1_2	3455	0.6	0.03	2.13	0.16	0.19	0.14	-64.69	Inner bulge
BP1_3	3995	1.68	0.18	1.59	0.06	0.22	0.06	-44.42	Inner bulge
BP1_5	3956	0.69	-1.14	1.67	-0.12	0.53	0.6	-94.94	Inner halo
BP1_6	3739	1.24	0.23	1.85	0.09	0.29	0.04	-78.95	Inner bulge
BP1_7	3743	0.7	-0.65	1.8	0.16	0.18	0.44	5.84	Inner bulge
BP1_9	3460	0.62	0.06	2.23	0.12	0.16	0.13	205.70	Inner bulge

3.2. Stellar Parameters with Thin-disk Oxygen Assumption

As mentioned in the previous section, the main assumption in the parameter determination method is the oxygen abundance, [O/Fe], which is assigned an abundance value based on a thin- or thick-disk metallicity-dependent trend, following the [O/Fe] versus [Fe/H] trends in Amarsi et al. (2019). We have assumed that the inner bulge stars follow the thick-disk [O/Fe] trend based on several previous studies, while determining the stellar parameters. Here we carry out an exercise where we assume thin-disk [O/Fe] abundances instead, and redetermine the stellar parameters, even though there is no reason to believe that this should be the case. This leads to a decrease in [O/Fe] by 0.05-0.35 dex, which in turn results in decreases in T_{eff} by 50–150 K, $\log g$ by 0.1–0.25 dex, [Fe/H] by 0.0–0.15 dex, and $\xi_{\rm micro}$ by -0.05–0.2 km s⁻¹. The most metal-poor stars, BP1_7 and BP1_5, have the largest differences in [O/Fe], of 0.19 and 0.35 dex, respectively, and thus the largest differences in $T_{\rm eff}$ (100 and 150 K) and $\log g$ $(\sim 0.25 \text{ dex})$ as well.

Nandakumar et al. (2023a) showed that when the thin- or thick-disk population assumption is wrong, the Mg abundances determined based on the resulting stellar parameters can be used to catch any such misclassification. This is illustrated in Figure 7 in Nandakumar et al. (2023a), where the [Mg/Fe] abundances decrease further for the incorrectly classified thindisk star and increase further for the incorrectly classified thick-disk star. The Mg abundances determined for the six inner bulge stars and the halo interloper from the new sets of stellar parameters, with the assumption of [O/Fe] following the thin disk, are enhanced by 0.02–0.05 dex, and thus further confirm

our assumption of a thick-disk trend for [O/Fe] vs [Fe/H] while determining the stellar parameters.

3.3. Orbital Analysis

To confirm that the stars observed in the $(l, b) = (0^{\circ}, +1^{\circ})$ field belong to the bulge, we performed orbit calculations. We used the software package AGAMA (Vasiliev 2019) to integrate the orbit over 500 Myr. The gravitational potential used is composed of three components: a halo and a disk, both from MWPotential14 (Bovy 2015), and a bar/bulge from Launhardt et al. (2002). The latter, which is initially at an angle of $\alpha = 25^{\circ}$ from the line of sight toward the Galactic Center, is rotating clockwise with a pattern speed of about $\Omega_b = 40 \,\mathrm{km \, s^{-1} \, kpc^{-1}}$ (Portail et al. 2017). Among the initial conditions (i.e., position, proper motions, radial velocity, and distance) necessary to integrate the orbits, the position and proper motions come from the Gaia Early DR3 survey (Gaia Collaboration et al. 2016, 2021) and the radial velocities are determined based on the wavelength shift of known lines in the observed spectra with respect to their wavelengths in vacuum. We estimate the spectrophotometric distances as explained by Rojas-Arriagada et al. (2014) and Schultheis et al. (2017), using the stellar parameters T_{eff} , $\log g$, and [Fe/H] and the nearinfrared photometry J, H, and K and associated errors. The coordinates of the orbits as a function of time and the orbital parameters, like the apocentric radius R_{max} and the maximum height from the Galactic plane z_{max} , allow us to determine the bulge membership.

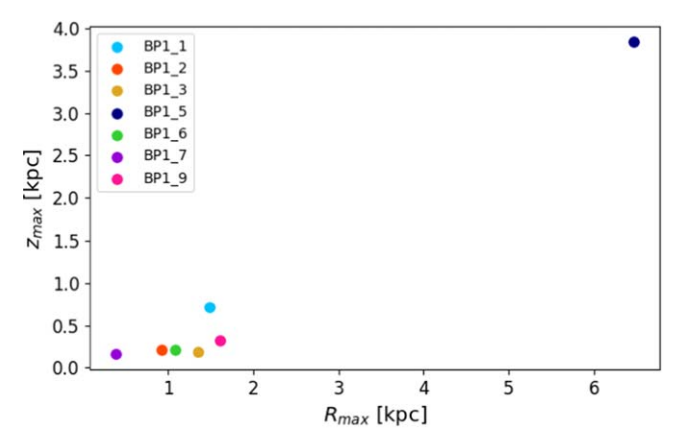


Figure 3. Maximal height from the Galactic plane z_{max} vs. apocentric radius R_{max} diagram for the seven M giants of the the $(l, b) = (0^{\circ}, +1^{\circ})$ field.

4. Results

In Figure 2, we plot the orbits for the seven stars observed at $(l, b) = (0^{\circ}, +1^{\circ})$. All stars except one are clearly members of the inner bulge and stay confined within a kiloparsec of the Galactic Center. The orbit calculation of the star BP1_5, however, shows that it more likely is a halo star passing by the center. We plot the maximum height from the Galactic plane z_{max} versus the apocentric radius R_{max} in Figure 3. In this figure, it is also obvious that we should exclude this star (BP1_5) from the discussion of the chemistry of stars in the inner bulge. The metallicity of this star ([Fe/H] = -1.14) is also more compatible with it being a halo star than an inner bulge star (see, for example, the discussion on the metallicity distribution of the inner bulge in Rojas-Arriagada et al. 2020). We have therefore marked this metal-poor star separately in the following discussion on the abundances versus metallicity.

We have thus determined the metallicities and abundances of 21 elements for the six inner bulge stars, one halo interloper, and the sample of 50 M giants in the solar neighborhood. For all elements except fluorine and cerium, we have scaled the abundances with respect to the solar abundance values from Grevesse et al. (2007). We used $A_{\odot}(F) = 4.43$ from Lodders (2003) and $A_{\odot}(Ce) = 1.58$ from Grevesse et al. (2015) for fluorine and cerium, respectively.

We classified the solar neighborhood M giants as belonging to the chemically defined thin- and thick-disk populations based on their enhanced APOGEE magnesium abundance from the [Mg/Fe] versus [Fe/H] plot and confirmed by our magnesium abundance determinations. In the following sections, we adopt the ideology from Haywood et al. (2013) while labeling the solar neighborhood stars as thin- and thick-disk, i.e., when we mention the thick disk and metal-rich thin disk, we refer to the inner disk sequence.

We show the observed and synthetic spectra of selected inner bulge stars for the absorption lines used in this work to determine the abundances of magnesium, silicon, sulfur, and calcium in Figure 4. The abundance trends are shown in Figure 5, with the inner bulge stars marked with black star symbols, the halo interloper with an orange star symbol, and the reference sample with red circles (low- α or thin-disk stars) and orange diamonds (high- α or thick-disk stars).

We estimate the uncertainties in the elemental abundances, shown as the error bars in Figure 5, for the star BP1_9. We redetermine 50 values of the abundances from all selected lines

of each element by setting the stellar parameters to values randomly chosen from normal distributions, with the actual stellar parameter value (listed in Table 2) as the mean and the typical uncertainties ($\pm 100\,\mathrm{K}$ in T_{eff} , $\pm 0.2\,\mathrm{dex}$ in $\log g$, $\pm 0.1\,\mathrm{dex}$ in [Fe/H], and $\pm 0.1\,\mathrm{km\,s^{-1}}$ in ξ_{micro}) as the standard deviation. The uncertainty in the abundance determined from each line is then taken to be the mid value of the difference between the 84th and 16th percentiles of the abundance distribution. The final abundance uncertainty is the standard error of the mean of the uncertainties from all chosen lines of an element. The estimated uncertainties are in the range of 0.05– $0.14\,\mathrm{dex}$ for all elements except sulfur, for which we estimate a larger uncertainty of $0.2\,\mathrm{dex}$. We carry out the same exercise for a typical solar metallicity star in the solar neighborhood reference sample and we get similar abundance uncertainties.

The metallicities of the stars were determined as one of the stellar parameters. Although we only have very few stars in the inner bulge set, their distribution in metallicity fits well in the emerging picture from Schultheis et al. (2015), Ryde et al. (2016), Nandakumar et al. (2018), and Nieuwmunster et al. (2023). Five of our stars fit the metal-rich peak, and the metal-poor star fits within the subsolar peak found in these other studies too. The metal-rich peak increases in relative terms, getting progressively more dominant, the closer to the plane the field lies (Nandakumar et al. 2018).

Next, we will compare the element ratio trends versus metallicity for the 21 elements determined for the inner bulge population and compare them differentially with those of the reference sample of stars in the local disks.

4.1. Fluorine (F)

Fluorine. The fluorine abundances are determined from six HF molecular lines in the K band; see Nandakumar et al. (2023b). For the solar neighborhood sample (also presented in Nandakumar et al. 2023b), we find a flat [F/Fe] versus [Fe/H] trend, but a hint of a slightly higher level of [F/Fe] for stars with [Fe/H] > 0 dex. In comparison, the five metal-rich, inner bulge stars have even higher derived [F/Fe] abundances. For stars with several useful lines, all the lines yield elevated F abundances, ensuring a precise derived mean abundance. The spectra are of good quality for all lines, and they are all abundance-sensitive and therefore not saturated. Our finding is therefore interesting, but due to the temperature sensitivity of the lines, more stars are needed in order to draw any firm conclusions. No reliable fluorine abundances could be derived for the metal-poor, inner bulge star, due to noisy spectra and the fact that telluric lines severely affected the HF lines for this star.

Magnesium, silicon, and calcium There is a clear enhancement in the mean abundances of the three α elements, Mg, Si, and Ca for the solar neighborhood, thick-disk stars, leading to a separation between the thin- and thick-disk populations. The metal-poor, inner bulge star shows similar enhancements to those shown by the thick-disk stars for these α elements. The rest of the five metal-rich, inner bulge stars also have enhanced abundances in the cases of Mg and Ca compared to the metal-rich, thin-disk stars and lie close to the upper envelope of the thin-disk abundance trend. In the case of Si, the mean

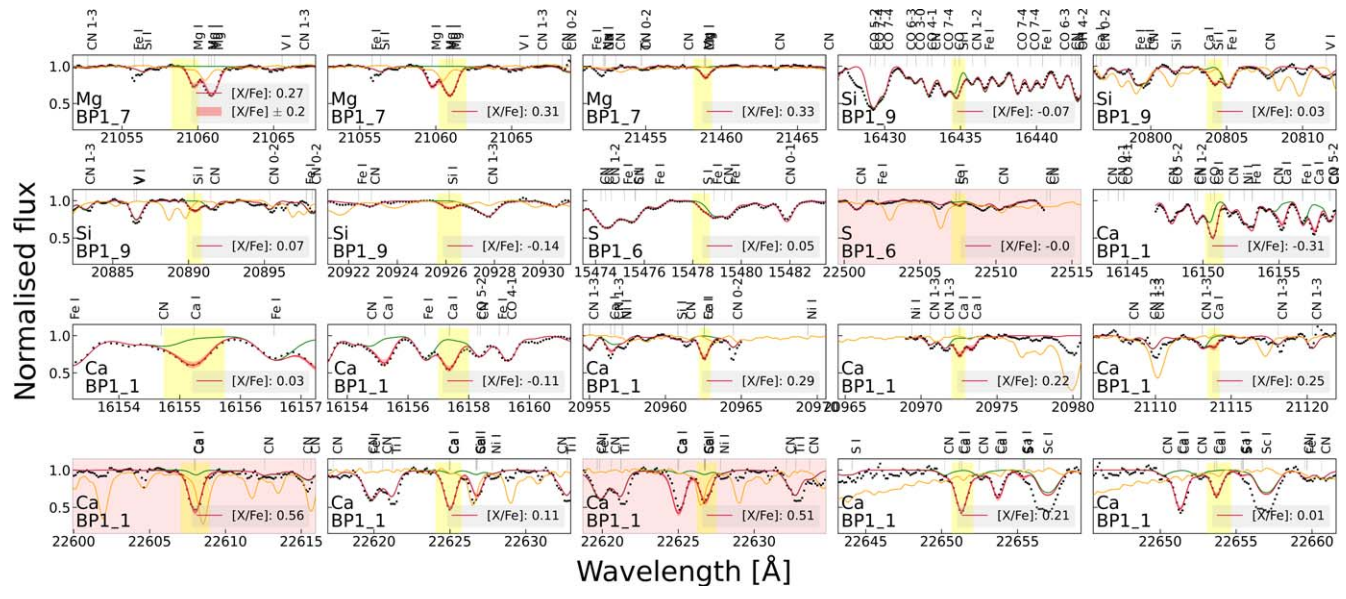


Figure 4. Wavelength regions centered at the three selected magnesium lines for the star BP1_7, the four selected silicon lines for the star BP1_9, the two selected sulfur lines for the star BP1_6, and the 11 selected calcium lines for the star BP1_1. In each panel, the black circles denote the observed spectrum, the crimson line denotes the best-fit synthetic spectrum, and the red band denotes the variation in the synthetic spectrum for a difference of ± 0.2 dex in the abundances. The yellow bands in each panel represent the line masks defined for each line, wherein SME fits the observed spectra by varying the elemental abundance and finding the best synthetic spectra fit by χ^2 minimization. The green line shows the synthetic spectrum without the absorption from the element, also indicating any possible blends in the line. The abundance values corresponding to the best-fit case for each line are listed in each panel. All identified atomic and molecular lines are also denoted at the top of each panel. The panels with red background correspond to the lines we have avoided due to bad noisy spectra or strong telluric contamination.

abundances for the metal-rich, inner bulge stars overlap with the metal-rich, thin-disk abundance trend. Overall, we find clear enhancements in the α -element abundances for the inner bulge stars that are consistent with the enhancement seen for the thick-disk stellar population.

Sulfur. The sulfur abundance determination is hampered by large uncertainties and therefore a large scatter in the abundance trends. We could only determine a reliable abundance from one weak H-band line for the inner bulge stars, since the K-band line is severely affected by telluric lines. The metal-poor, halo interloper star (BP1_5) shows an expected elevated [S/Fe] abundance ratio, whereas the metal-poor, inner bulge star shows a lower sulfur abundance. As mentioned earlier, the uncertainties in the sulfur determination $(\pm 0.2 \, \text{dex})$ are, however, largest for all the elements. The scatter in abundances for the solar neighborhood stars is also more prominent at lower metallicities (see also Figure 7). We would need a larger sample of inner bulge stars in this metallicity regime to discern whether it follows the thick disk or not.

4.3. Odd-Z Elements (Na, Al, and K)

Sodium. The mean [Na/Fe] trend for the solar neighborhood sample resembles a stretched out N shape (cf. Bensby et al. 2014). The trend for the metal-poor, thick-disk stars shows a hint of a separate trend compared to that of the thin-disk stars, following the upper envelope of the thin-disk trend. The [Na/Fe] values determined for the metal-poor, inner bulge star (BP1_7) cannot be differentiated from either disk trend in the solar neighborhood. The five metal-rich, inner bulge stars overlap with the solar neighborhood trend.

Aluminum. The mean [Al/Fe] of the solar neighborhood, thin-disk stars is generally near solar (in the supersolar regime).

The [Al/Fe] values of the thick-disk stars are enhanced by $\sim\!\!0.2$ dex, and decrease as metallicity decreases, which is also expected from chemical evolution models (see, for example, Kobayashi et al. 2020). The mean [Al/Fe] for the metal-poor, inner bulge star is consistent with the thick-disk trend. The mean [Al/Fe] values of the metal-rich, inner bulge stars roughly follow the solar neighborhood disk population trend, perhaps with a tendency of following an upper envelope.

Potassium. For the metal-poor, thick-disk stars, there is a clear enhancement in [K/Fe]. The mean [K/Fe] values for the thin-disk stars are slightly subsolar and show a near-straight trend. Only four inner bulge stars have reliable [K/Fe] determined from good-quality lines in their spectra. Three of them are metal-rich and have mean abundance values at the upper envelope of the trend of the solar neighborhood metal-rich, thin-disk stars. The enhanced abundance of the metal-poor, inner bulge star (BP1_7) is consistent with the enhanced values of the solar neighborhood metal-poor, thick-disk stars.

4.4. Iron-peak Elements (Sc, Ti, V, Cr, Mn, Co, and Ni)

Scandium. The mean [Sc/Fe] trend in the solar neighborhood shows a generally decreasing slope with metallicity, with the thick-disk stars showing higher Sc abundances than those of the thin disk. The metal-poor, inner bulge star (BP1_7) follows the thick-disk trend and the metal-rich ones follow the solar neighborhood metal-rich, thin-disk trend. These show a similar spread in abundance for a given metallicity. These lines are temperature sensitive (see, e.g., Thorsbro et al. 2018), which could be the cause of the large spread.

Titanium. The thick-disk trend of [Ti/Fe] is clearly separated from that of the thin disk for the solar neighborhood stars. The metal-poor, inner bulge star (BP1_7) shows a similar enhancement as the thick-disk stars. The rest of the five metal-rich,

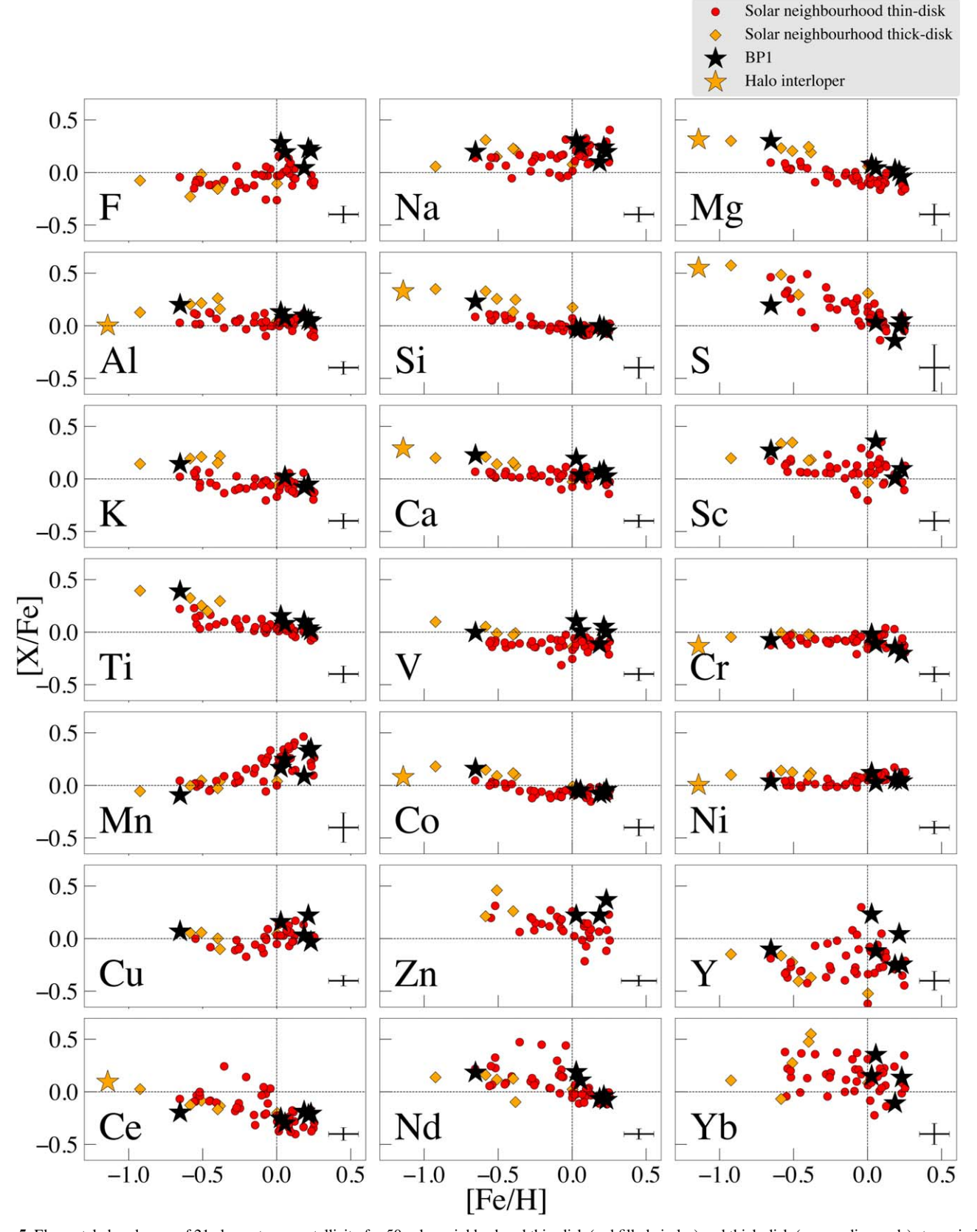


Figure 5. Elemental abundances of 21 elements vs. metallicity for 50 solar neighborhood thin-disk (red filled circles) and thick-disk (orange diamonds) stars, six inner bulge stars (black stars), and the halo interloper (orange star). Elemental abundances are the mean values determined from multiple lines for all elements, except V, Co, Zn, and Yb.

inner bulge stars also have slightly enhanced abundances compared to the metal-rich, thin-disk stars and lie close to the upper envelope of the metal-rich, thin-disk abundance trend.

Vanadium. The thin-disk stars have subsolar values of [V/Fe] and the metal-poor, thick-disk stars have enhanced supersolar values in the solar neighborhood and show a flat trend. The metal-poor, inner bulge star (BP1_7) shows a similar enhancement as the thick-disk stars. The rest of the five metal-rich, inner bulge stars also have slightly enhanced abundances compared to the metal-rich, thin-disk stars and lie close to the upper envelope of the metal-rich, thin-disk abundance trend.

Chromium. The mean [Cr/Fe] values for the solar neighborhood stars are mainly subsolar at all metallicities, with larger scatter for metal-rich stars. Overall, this shows an expected flat trend for Cr (e.g., Bensby et al. 2017). The abundance differences between the thin- and thick-disk stars are small, although the metal-poor, thick-disk stars show a consistent enhancement in [Cr/Fe] compared to the thin-disk stars from all three lines used to determine the abundances. The measured mean abundance for all six inner bulge stars is consistent with the solar neighborhood trend. We cannot rule out that the metal-poor, inner bulge stars follow the thick-disk trend.

Manganese. Based on the discussion in Nandakumar et al. (2024), showing that Mn empirically is more like a normal iron-peak element, there are reasons to believe that the [Mn/Fe] versus [Fe/H] trend in the solar neighborhood is essentially flat. The non-LTE corrections for the M giants analyzed here are, therefore, most likely underestimated for the highest metallicities. However, when comparing the solar neighborhood populations and the inner bulge stars, we are only interested in the differential differences between the populations' trends and not so much their absolute values. The [Mn/Fe] trend of the inner bulge stars nicely follows the solar neighborhood one.

Cobalt. The trend for the thin-disk, solar neighborhood stars for [Co/Fe] starts with supersolar values at lowest metallicities that transition to subsolar values at $[Fe/H] \sim -0.4 \, dex$ and continue at subsolar values as the metallicity increases. All five metal-poor, thick-disk stars have enhanced [Co/Fe] values, and the solar metallicity thick-disk star has a solar [Co/Fe] value that is closer to the thin-disk stars. The thin- and thick-disk trends are clearly separated. Similar enhancement in [Co/Fe] as for the thick-disk stars is found for the metal-poor, inner bulge star (BP1_7), while the five metal-rich, inner bulge stars follow the metal-rich, thin-disk abundances.

Nickel. The mean [Ni/Fe] values for the thin-disk stars show a tight trend that increases slightly with increasing metallicity. The thick-disk stars show enhancements with supersolar values. The [Ni/Fe] values for the metal-poor, inner bulge star (BP1_7) follow the disk trends and those of the five metal-rich, inner bulge stars are consistent with the solar neighborhood trend.

4.5. Transition Elements between Iron-peak and Neutroncapture Elements (Zn)

Zinc. The abundance trend of [Zn/Fe] resembles an α element, decreasing with metallicity and with the thick-disk trend higher than that of the thin-disk trend. We could determine the [Zn/Fe] abundances for only three metal-rich stars in the inner bulge, and they are consistent with the solar

neighborhood values in the supersolar metallicity range, tending to follow the upper envelope.

4.6. Neutron-capture Elements (Cu, Zn, Y, Ce, Nd, and Yb)

We have determined the abundances of copper (Cu), yttrium (Y), cerium (Ce), neodymium (Nd), and ytterbium (Yb), which are all mainly synthesized by neutron-capture processes. Cu is synthesized through the weak s-process in massive stars (e.g., Pignatari et al. 2010; Ernandes et al. 2020; Baratella et al. 2021). Most neutron-capture elements are produced by a combination of the s- and r-processes. For Y and Ce, the s-process dominates, with s/r = 70/30 and 85/15, respectively, in the solar isotopic mixture (Bisterzo et al. 2014; Prantzos et al. 2020). Neodymium has a 60/40 ratio and can therefore still be considered as predominantly an s-process element. The more the *r*-process contributes, the more the abundance trends will resemble and reveal an r-process contribution. On the other hand, ytterbium has a ratio close to 50/50 (Bisterzo et al. 2014; Kobayashi et al. 2020; Prantzos et al. 2020), which makes Yb the most r-process-rich element among the elements we are investigating.

4.6.1. Weak s-process Elements (Cu)

Copper. The mean [Cu/Fe] abundances for the solar neighborhood stars show a wavelike trend, starting off at slightly supersolar values at the lowest metallicities, then decreasing to subsolar values at subsolar metallicities, but then again increasing at supersolar metallicities. The thick-disk stars tend to lie above those of the thin disk.

The inner bulge stars follow these trends nicely, following the thick disk and then being consistent with the solar neighborhood [Cu/Fe] values at supersolar metallicities.

4.6.2. s-process-dominated Elements (Y, Ce, and Nd)

Yttrium. The derived [Y/Fe] abundances determined for the solar neighborhood sample show subsolar values and scatter for values at a given metallicity for the thin disk. The thick-disk stars have [Y/Fe] values that follow the lower envelope of the thin-disk trend. The six inner bulge stars have scattered [Y/Fe] values consistent with the solar neighborhood [Y/Fe] trend and range.

Cerium. Just like in the case of the trend for yttrium, the thick-disk stars follow the lower envelope of the thin-disk trend for the solar neighborhood stars (see, e.g., Forsberg 2023). The trend from all six inner bulge stars is consistent with the solar neighborhood, thick-disk [Ce/Fe] trend for low metallicities, and follows the general solar neighborhood trend for the metal-rich stars.

Neodymium. The [Nd/Fe] determinations for the thick-disk stars in the solar neighborhood sample again follow the lower envelope of the thin disk. The inner bulge stars follow the solar neighborhood trend.

4.6.3. Element with 50/50 s- and r-process Contributions (Yb)

Ytterbium. There is a large scatter (\sim 0.5 dex) in the [Yb/Fe] values for the solar neighborhood populations. Although there is a large scatter, the general picture that the thick-disk and the thin-disk [Yb/Fe] values more or less overlap is very similar to what Forsberg (2023) finds for praseodymium, Pr. This element too has a 50/50 contribution of s- and p-process origins in the

solar isotopic mixture (Bisterzo et al. 2014). We could determine the [Yb/Fe] abundances for only four metal-rich stars in the inner bulge, and they are consistent with the solar neighborhood values in the supersolar metallicity range.

5. Discussion

Chemodynamic characterization of the stellar populations in the inner bulge is essential for disentangling their formation and evolutionary scenarios. They have, however, escaped a detailed chemical study, due to the dust extinction along the line of sight. A differential chemical study comparing the inner bulge populations with those in the solar neighborhood would reveal similarities and differences in the environmental influences on, for example, the star formation histories and processes, gas-flow patterns, evolutionary timescales, and stellar evolutionary processes in the different populations (see, e.g., Friske & Schönrich 2023).

5.1. The Bulge

The large structure referred to as the Milky Way bulge (within 10° of the Galactic Center; Barbuy et al. 2018) has successfully been chemically investigated in recent years. At least two components in the metallicity distribution function are found in previous studies (e.g., Hill et al. 2011; Rojas-Arriagada et al. 2017, 2020; Johnson et al. 2022), with a consensus on the metal-rich peak at $\sim +0.3$ dex being associated with the barred bulge. The physical origins and the number of metal-poor peaks is, however, debated (Bland-Hawthorn & Gerhard 2016; Rojas-Arriagada et al. 2020; Johnson et al. 2022).

There is a consensus that the chemistry of the stars in the bulge is similar to that of the local thick disk when it comes to the α elements, such as Mg, Si, and Ca (Meléndez et al. 2008; Ryde et al. 2010; Johnson et al. 2014; Bensby et al. 2017; Jönsson et al. 2017; Lomaeva et al. 2019; Nieuwmunster et al. 2023), or at least following the upper envelope of the thick-disk trends. These elements are good probes for modeling the star formation history of a stellar population (see, e.g., Grisoni et al. 2017; Matteucci 2021).

For the emerging picture with the bulge being the bar seen edge-on, these trends might be expected if the general picture of the α trends is extrapolated inward from the findings from the APOGEE survey (Hayden et al. 2015; Queiroz et al. 2020). These trends show a thick disk dominating, with a small scale length and a metal-rich disk with low α that is getting progressively more metal-rich the smaller the galactocentric radius, reflecting the metallicity gradient.

5.2. The Inner Bulge

Chemical studies of the stellar populations in the inner bulge regions ($|b| < 2^{\circ}$, or $\sim \pm 300$ pc in projected distance from the Galactic Center) are, however, sparse. A few chemical studies have revealed an α -element trend versus metallicity, again resembling that of the local thick disk (e.g., Schultheis et al. 2020; Nieuwmunster et al. 2023). The Mg, Si, and Ca trends in Nieuwmunster et al. (2023) follow the thick-disk trends but sample more of the most metal-rich stars, a fact that was already seen in Ryde & Schultheis (2015) with a metal-rich population with thick-disk α trends in the Galactic Center populations. The stars investigated in Schultheis et al. (2020),

situated within 150 pc of the Galactic Center, show similar Mg, Si, Ca, and O trends to the Galactic bulge.

The very inner region, the region within 200 pc ((|b| < 1°,5), is dominated by the NSD, whose chemical history might be expected to be different, depending on the formation scenario. We can assume that the NSD could have had intense star formation dominated by outward-moving star-forming regions (Friske & Schönrich 2023). These regions have been in the form of nuclear rings, which have been fed by strong gas inflows driven by the surrounding bar and funnelled from the bar tips (Friske & Schönrich 2023). Different inflow scenarios distribute heavy elements very differently in the NSD, with a possible pileup toward the inner radial parts of the NSD (for predictions, see Friske & Schönrich 2023).

The NSD is a flattened structure with a stellar density profile that falls off rapidly (see Nishiyama et al. 2013; Wegg & Gerhard 2013; Bland-Hawthorn & Gerhard 2016). Our stars presented here all lie in a field along the northern minor axis at $(l=0^{\circ}, b=+1^{\circ})$, which is too far away from the plane to be considered as belonging to the NSD. Our six stars can, therefore, be considered to be in the inner bulge, but not in any of the inner structures found there, especially the NSD. Stars closer to the center, in the NSD and NSC, will be presented in a forthcoming paper.

A dimension that is lacking in earlier discussions involves the elemental trends from species other than the α elements. All elements are formed from a unique mixture of different nucleosynthetic networks, acting at vastly different timescales. Therefore, by investigating a range of elements belonging to different classes of elements, new insights can be gained. The neutron-capture elements especially are distinct from the lighter elements. Manea et al. (2023) illustrate clearly the importance of considering the neutron-capture elements when chemically characterizing stars. Among the 21 elements we have investigated here for the inner bulge stars, we have representatives of the α , odd-Z, iron-peak, transition elements between iron-peak and neutron-capture elements, neutron-capture elements (i.e., weak s-process, s-process-dominated elements, and r-process-dominated elements), and fluorine, with its unique formation history (Ryde et al. 2020).

Overall, we find a clear similarity and consistency between the element trends for all 21 elements, beside that of fluorine, for the stellar populations in the inner bulge, on one hand, and the local thick-disk and metal-rich thin disk (inner disk sequence), on the other. The enhancements in the α -element abundances, as well as in the Al, K, Sc, Ti, Co and V abundances, are strikingly similar for the metal-poor stars, following the local thick-disk trends. These elements mostly also follow the upper envelope of the local thin disk at high metallicities. These similarities and consistencies are also found in the s-process-dominated elements Y and Ce, where the thick-disk trends follow the lower envelope of the thin-disk scatter or "cloud" at -0.5 < [Fe/H] < 0; see Nandakumar et al. (2024). Also, the weak s-process element, Cu, shows a great similarity between the stars in the local thick-disk and inner bulge stars. Nd also has a dominant s-process origin, but to a lesser degree than for Ce. The trends for the stars in the inner bulge and the local thick disk are consistent with coming from a similar population for Nd also. These facts all strengthen the similarity between the inner bulge and the local thick disk in a new dimension, namely the neutron-capture dimension (Manea et al. 2023). There is also a large similarity between the trends

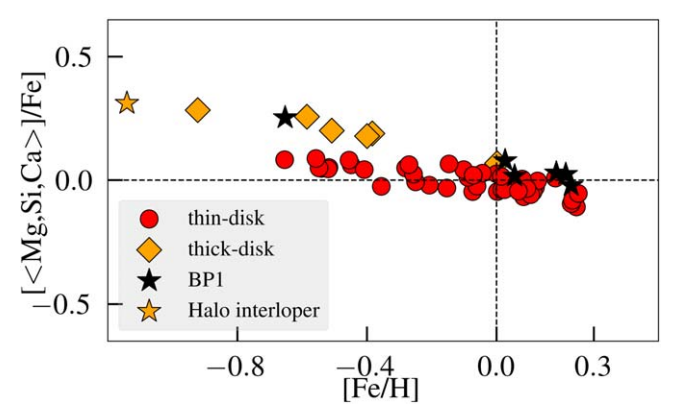


Figure 6. Mean abundances of the three α elements, Mg, Si, and Ca, vs. [Fe/H] for 50 M giants in the solar neighborhood reference sample (red circles and orange diamonds) and the seven inner bulge stars (black stars).

for the iron-peak elements (Cr, Mn, and Ni) of the inner bulge stars and the solar neighborhood stars. In summary, the hypothesis that the two populations are chemically similar can, therefore, not be rejected.

In Figure 6, we show the similarity between the local thick disk, plotted with orange diamonds for a mean of the three well-determined α elements (Mg, Si, and Ca), and the inner bulge stars, plotted as black stars. The metal-rich inner bulge stars follow the upper envelope of the local metal-rich thin disk. The precision of the data is also clear in the plot. Using the cosmological zoom simulation VINTERGATAN (Agertz et al. 2021), Renaud et al. (2021) demonstrated that an upper envelope in $[\alpha/Fe]$ trends can be associated with star formation in dense gas clouds where star formation is "fast," i.e., with short gas depletion times (see also Clarke et al. 2019). In these dense environments, stellar feedback is less efficient at disrupting the natal clouds, leading to α -rich ejecta from core-collapse supernovae rapidly being reincorporated into the star formation process, hence enhancing $[\alpha/Fe]$ in newly formed stellar populations at a relatively constant [Fe/H]. It remains to be understood whether the enhancement in our metal-rich sample of stars (see also Thorsbro et al. 2020) reflects the past star formation conditions of the inner bulge, or whether this population of stars formed at greater galactocentric radii in massive dense gas clouds that migrated to the center due to dynamical friction (e.g., Immeli et al. 2004; Elmegreen et al. 2008; Agertz et al. 2009).

The only clear differences between the populations are (i) the distribution of the metallicities of the stellar populations being more metal-rich in the inner bulge regions and (ii) the fluorine trend with metallicity. We refrain from drawing any conclusions from the higher fluorine trend at high metallicities, due to the temperature-sensitive nature of the lines. A large set of stars in the inner bulge region for a range of metallicities would be needed to draw more conclusions. However, an explanation that would increase the fluorine trend at higher metallicities, and especially at supersolar metallicities, is a contribution to the cosmic budget for fluorine from novae, as suggested by Spitoni et al. (2018). This process increases its yields with metallicity at supersolar metallicities (see models in Ryde et al. 2020). Whether or not novae could contribute at supersolar metallicities is currently not known, since the novae yields are highly uncertain (Spitoni et al. 2018).

We also determined abundances of all 21 elements with the new sets of stellar parameters determined with the thin-disk oxygen assumption, as described in the Section 3.2. This provides us with an estimate of the abundance variations due to the change in stellar parameters from oxygen assumption. For the metal-rich stars ([Fe/H] > 0), Mg, Al, Si, Ca, Zn, and Yb exhibit the smallest difference (<0.06 dex), and the rest of the elements have differences less than 0.18 dex. The most metalpoor star, BP1_5, with the largest difference in $T_{\rm eff}$ (150 K) and $\log g$ (0.25 dex), exhibits a difference of \sim 0.27 dex for cerium and much lower differences ($<0.18 \,\mathrm{dex}$) for all other elements. The largest differences in the cases of metal-rich stars are found for fluorine (0.18 dex) and scandium (0.14 dex). This can, indeed, be attributed to the $T_{\rm eff}$ -sensitivity of the HF and ScI lines, from which we determined the abundances (see also Sections 4.1 and 4.4). Such large differences would make the fluorine abundances consistent with the local thin-disk abundances, hence the reason for refraining from drawing any conclusions from the higher fluorine trend at high metallicities.

5.3. Comparison with Inner Milky Way Stars

Next, we compare our abundance trends with those from the inner Milky Way stellar sample of Zasowski et al. (2019), but using the abundances provided in the APOGEE DR17 catalog. We also include the Mg, Si, and Ca abundance trends determined from CRIRES K-band spectra for 16 K and M giants in the $(l, b) = (0^{\circ}, +1^{\circ})$ field in Nieuwmunster et al. (2023).

Zasowski et al. (2019) selected \sim 4000 stars with 3600 K \leq Teff \leq 4500 K and $-0.75 \leq$ log $g \leq$ 3.5 in APOGEE DR14/DR15 that are at galactocentric distances, $R \leq$ 4.0 kpc, and investigated the elemental abundance trends of 11 elements. We thus selected the same set of stars from the APOGEE DR17 catalog and compared our elemental abundance trends for 14 elements (three more are available in APOGEE DR17) in Figure 7, where the Mg, Si, and Ca abundance trends from Nieuwmunster et al. (2023), mentioned above, are also plotted.

Zasowski et al. (2019) found a lack of bimodality in the $\lfloor \alpha/\mathrm{Fe} \rfloor$ distributions at subsolar metallicity, suggesting that the abundances are dominated by a single chemical evolutionary sequence. They also found inner Milky Way abundances for several non- α elements to be similar to the solar radius stars in APOGEE that belong to the high- α ($\lfloor \alpha/\mathrm{M} \rfloor > 0.12$) sample. Our findings agree with this, and more importantly we add more chemical species from other nucleosynthetic channels, not investigated before in the inner bulge region. We show that the trends of these newly added elements also exhibit values similar to the solar neighborhood thick-disk stars.

In Figure 7, we find excellent agreements in the cases of elements with the least scatter in APOGEE: Mg, Si, Ca, and Ni. Both Na and S in APOGEE show good agreement with our abundance values, though APOGEE shows large scatter at subsolar metallicities. Significant differences are seen for Ti, V, Cr, and Mn. Our Ti abundances are significantly better and agree with the predictions from theoretical chemical evolution models compared to the N-shaped trend in APOGEE. We also note that Hawkins et al. (2016) have improved the abundance ratios of [Ti/Fe] and [V/Fe] (with respect to those in APOGEE DR12) with the reanalysis of APOGEE spectra using the BACCHUS pipeline through careful line selection. For Mn, we have used NLTE corrections based on calculations by Amarsi et al. (2020), whereas NLTE corrections for Mn are not

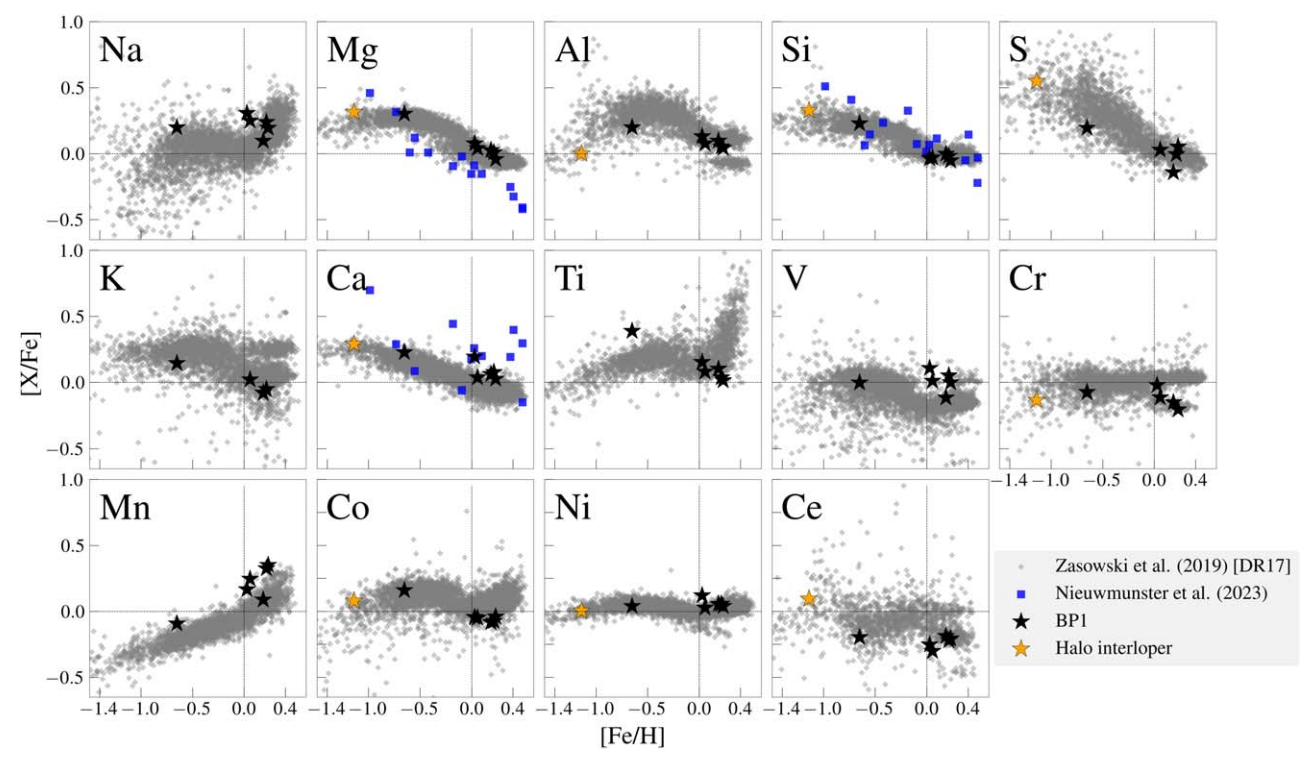


Figure 7. Elemental abundances of 14 elements vs. metallicity for inner Milky Way stars (gray squares) investigated in Zasowski et al. (2019) selected from the APOGEE DR17 catalog and inner bulge stars in this work (black star markers). The abundances of Mg, Si, and Ca for stars located in the BP1 field in Nieuwmunster et al. (2023) are shown as blue squares.

included in APOGEE. We have also included hyperfine splitting information for the Mn lines from Montelius (2021), while it is not clear whether the APOGEE line list includes this information for Mn. For Al, K, and Cr, there is a bifurcation at high metallicities for APOGEE, and Zasowski et al. (2019) have shown that Al, K, Cr, Mn, and Co in APOGEE DR14/ DR15 exhibit $T_{\rm eff}$ dependencies for stars with $T_{\rm eff}$ < 3800 K. We note that we do not see $T_{\rm eff}$ dependence for these elements based on the comparison of our solar neighborhood reference sample trends with the elemental trends from the GILD survey (H. Jönsson et al., in preparation), which is an optical survey of ~500 warmer K giants in the solar neighborhood (Nandakumar et al. 2024). In the case of Ce, our inner bulge abundances lie in the lower envelope of the APOGEE Ce trend, but they are consistent with the solar neighborhood reference sample, as shown in Figure 5. This difference in Ce abundances could be due to the choice of different Ce II lines in APOGEE and this work or due to the systematic differences in stellar parameters (see the following paragraph).

In general, most of the disagreements/differences with APOGEE may be attributed to a combination of different factors, like differences in spectral resolution, careful line selection, line lists, pipelines, etc. As mentioned before, this has been shown in Hawkins et al. (2016) and Hayes et al. (2022), where they reanalyze APOGEE spectra using the independent pipeline BACCHUS along with an improved line list and careful line selection. This has improved the abundance trends of elements like Na, Ti, S, V, and Ce and has led to measuring elements that APOGEE fails, such as P, Cu, and Nd. In this work, we determine stellar parameters self-consistently by spectral synthesis from IGRINS spectra using SME. A comparison between our stellar parameters and those from APOGEE for 44 solar neighborhood stars, which are also in

APOGEE, in Nandakumar et al. (2023a), has shown that there are systematic differences of $\sim\!100\,\mathrm{K}$ in T_{eff} , 0.3 dex in $\log g$, and 0.2 km s $^{-1}$ in ξ_{micro} . This could in turn lead to systematic differences in elemental abundances. Furthermore, for elements such as Mg, Ca, S, Ti, and Ni, we were able to choose more lines from the K band, owing to the broader wavelength coverage of IGRINS spectra (full H and K bands). This could also lead to differences in the abundance trends between this work and APOGEE. In addition, IGRINS has nearly two times higher resolution than APOGEE. This is crucial in capturing blends and uncertain continua in the crowded spectra of cool metal-rich stars and thus leads to more accurate abundances from IGRINS spectra.

Nieuwmunster et al. (2023) determined the three α -element abundances from the few K-band lines available in CRIRES spectra. Though both our work and Nieuwmunster et al. (2023) use the same line list, there are only two Mg and Ca lines and three Si lines in common between our work and that of Nieuwmunster et al. (2023). While there is significant scatter in the Si abundances for stars in Nieuwmunster et al. (2023), there is generally a good agreement with the abundances of our stars. The Mg abundances have the least scatter but are lower compared to our abundances. The Ca abundances in Nieuwmunster et al. (2023) are elevated for the supersolar metallicities and there is a large scatter as well. When we determine the Mg and Ca abundances from the same two lines used in Nieuwmunster et al. (2023), the Mg abundances decrease (see also Figure 9 in Nandakumar et al. 2023a) and the Ca abundances increase for the supersolar metallicity stars in our sample, consistent with Nieuwmunster et al. (2023). Hence, in addition to self-consistently determining stellar parameters from the same spectra, the ability to choose better H- and Kband lines has improved the abundances in this work. This

emphasizes the importance of an instrument like IGRINS, which covers the full *H*- and *K*-band wavelength regimes, in spectroscopic studies of stellar populations in the Milky Way.

6. Conclusions

The chemical evolution of the Galactic bulge as a function of Galactic latitude is of great interest for the study of the Milky Way, and the problem is likely to be one of increasing complexity as sample sizes, and numbers of elements, increase. Especially, the inner, dust-obscured regions, where most of the mass lies, hold important and likely interesting information. The innermost degree also contains the Central Molecular Zone, the NSD, and the NSC, as well as the stellar density peak of the inner stellar halo. In some of these locations, star formation may be ongoing, and stars formed within the last few Gyr may contribute to the population (see, e.g., Thorsbro et al. 2023). These regions have, however, not been chemically explored much, due to heavy optical extinction along the line of sight. To disentangle these different structures, a chemical characterization of the stellar populations there is needed. Infrared spectroscopic data at the highest quality and spectral resolution are required to achieve high precision and accuracy. IGRINS meets these requirements, observing the full H and K bands.

Taking advantage of the extraordinarily high spectral resolution and wavelength range of IGRINS, we present a spectral analysis and the first heavy element trends, and fluorine measurements, for seven M giants lying at (l, b) = $(0^{\circ}, +1^{\circ})$. Six stars in our sample are inner bulge stars, probably in the vicinity of, but not in, the NSD. We present a differential investigation of 21 elemental trends versus metallicity at high precision. We compare with derived abundances for stars in the solar neighborhood region of the same spectral type (here, M giants). In order to be strictly differential and minimize any systematic uncertainties, we use the same instrument with the same wavelength range, spectral resolution, pipelines, and analysis techniques in the determination of the stellar parameters and elemental abundances. The large number of elements offers new dimensions in chemical space, beyond the metallicity and the commonly studied α elements. This provides new insights (see, e.g., Manea et al. 2023) and potentially can break degeneracies. There will be a tension among results, as detailed analyses based on spectrum synthesis of individual spectra bump up against the results of very large programs.

We find that the stars in the inner bulge, 1° north of the Galactic Center, are strikingly homogeneous with the local thick disk (i.e., the solar neighborhood "inner disk sequence," as referred to by Haywood et al. 2013) in the chemical trends for 21 of the elements, which include all nucleosynthetic channels, i.e., α , odd-Z, iron-peak, transition elements between iron-peak and neutron-capture elements, and neutron-capture elements (i.e., weak-s, s-process-dominated elements, and r-process-dominated elements). The hypothesis that the two populations are similar chemically cannot be rejected.

The only clear differences between the populations are, first, that we note that we are efficiently detecting metal-rich stars in the inner bulge regions and fewer stars at medium metallicities, and, second, that the fluorine trend with metallicity *could be* different from the trend in the solar neighborhood. Although, prematurely, we can note that a way to increase the fluorine abundance in a stellar population is by the contributions to the

cosmic budget for fluorine from novae, as suggested by Spitoni et al. (2018). Whether this would indeed be the case is very unclear, since the nova yields are highly uncertain (Spitoni et al. 2018). In any case, the fluorine trend needs more attention and a more robust trend needs to be established for the stellar populations in the inner bulge structures. We also note that among the few stars we observe in the inner bulge, we have observed only one metal-poor star out of all six stars ([Fe/H] < -0.5).

We have demonstrated that a precise abundance analysis of as many as 21 elements of stars in the inner bulge is possible with the IGRINS spectrometer. The remarkable capabilities of this instrument—access to both the H and K infrared bands, with complete spectral coverage at resolution R=45,000—will not be matched by the next generation of large-scale infrared high-resolution spectroscopy surveys, which utilize only the H band at resolution R=18,000-23,000. For these next-generation surveys, the study of a number of interesting heavy elements, and fluorine, will be impossible. Our investigation emphasizes the need for continued work on these very interesting inner galaxy populations using the currently most powerful infrared spectrograph for high-resolution spectroscopy, IGRINS.

Our data presented here were observed with 2.7 m (107 inch) Harlan J. Smith Telescope at the McDonald Observatory in 2016 May–July. The next step is to observe the structures in the Galactic Center region, which is possible with larger telescopes. A forthcoming paper will present 21 elemental trends for stars in the NSC.

Acknowledgments

We thank the anonymous referee for the constructive comments and suggestions that improved the quality of the paper. NR and GN are supported by the grant 2023-04744 from the Swedish Research Council. G.N. acknowledges the support from the Wenner-Gren Foundations (UPD2020-0191 and UPD2022-0059) and the Royal Physiographic Society in Lund through the Stiftelsen Walter Gyllenbergs fond. N.R. acknowledges support from the Royal Physiographic Society in Lund through the Stiftelsen Walter Gyllenbergs fond and Märta och Erik Holmbergs donation. O.A. acknowledges support from the Knut and Alice Wallenberg Foundation and the Swedish Research Council (grant 2019-04659). B.T. acknowledges the financial support from the Wenner-Gren Foundation (WGF2022-0041). E.A. acknowledges support from the US National Science Foundation under grants AST18-15461 and AST23-07950. This work used The Immersion Grating Infrared Spectrometer (IGRINS), which was developed under a collaboration between the University of Texas at Austin and the Korea Astronomy and Space Science Institute (KASI), with the financial support of the US National Science Foundation under grants AST-1229522, AST-1702267, and AST-1908892, the McDonald Observatory of the University of Texas at Austin, the Korean GMT Project of KASI, the Mt. Cuba Astronomical Foundation, and the Gemini Observatory. This work is based on observations obtained at the international Gemini Observatory, a program of NSF's NOIRLab, which is managed by the Association of Universities for Research in Astronomy (AURA) under a cooperative agreement with the National Science Foundation on behalf of the Gemini Observatory partnership: the National Science Foundation (United States), National Research Council (Canada), Agencia

Nacional de Investigación y Desarrollo (Chile), Ministerio de Ciencia, Tecnología e Innovación (Argentina), Ministério da Ciência, Tecnologia, Inovações e Comunicações (Brazil), and Korea Astronomy and Space Science Institute (Republic of Korea).

Facility: Smith.

Software: SME (Valenti & Piskunov 1996, 2012), IRAF (Tody 1993), TOPCAT (version 4.6; Taylor 2005); Python (version 3.8) and its packages ASTROPY (version 5.0; Astropy Collaboration et al. 2022), SCIPY (Virtanen et al. 2020), MATPLOTLIB (Hunter 2007) and NUMPY (van der Walt et al. 2011).

ORCID iDs

```
Govind Nandakumar https://orcid.org/0000-0002-6077-2059
Nils Ryde https://orcid.org/0000-0001-6294-3790
Gregory Mace https://orcid.org/0000-0001-7875-6391
Kyle F. Kaplan https://orcid.org/0000-0001-6909-3856
Niels Nieuwmunster https://orcid.org/0000-0002-4080-2927
Daniel Jaffe https://orcid.org/0000-0003-3577-3540
R. Michael Rich https://orcid.org/0000-0003-0427-8387
Mathias Schultheis https://orcid.org/0000-0002-6590-1657
Oscar Agertz https://orcid.org/0000-0002-4287-1088
Eric Andersson https://orcid.org/0000-0003-3479-4606
Christopher Sneden https://orcid.org/0000-0002-3456-5929
Brian Thorsbro https://orcid.org/0000-0002-5633-4400

References
```

```
Afşar, M., Bozkurt, Z., Topcu, G. B., et al. 2023, ApJ, 949, 86
Agertz, O., Renaud, F., Feltzing, S., et al. 2021, MNRAS, 503, 5826
Agertz, O., Teyssier, R., & Moore, B. 2009, MNRAS, 397, L64
Amarsi, A. M., Lind, K., Asplund, M., Barklem, P. S., & Collet, R. 2016,
   MNRAS, 463, 1518
Amarsi, A. M., Lind, K., Osorio, Y., et al. 2020, A&A, 642, A62
Amarsi, A. M., Nissen, P. E., & Skúladóttir, Á. 2019, A&A, 630, A104
Amarsi, A. M., Nordlander, T., Barklem, P. S., et al. 2018, A&A, 615, A139
Astropy Collaboration, Price-Whelan, A. M., & Lim, P. L. 2022, ApJ, 935, 167
Baratella, M., D'Orazi, V., Sheminova, V., et al. 2021, A&A, 653, A67
Barbuy, B., Chiappini, C., & Gerhard, O. 2018, ARA&A, 56, 223
Bensby, T., Feltzing, S., Gould, A., et al. 2017, A&A, 605, A89
Bensby, T., Feltzing, S., & Oey, M. S. 2014, A&A, 562, A71
Bisterzo, S., Travaglio, C., Gallino, R., Wiescher, M., & Käppeler, F. 2014,
   ApJ, 787, 10
Bland-Hawthorn, J., & Gerhard, O. 2016, ARA&A, 54, 529
Bovy, J. 2015, ApJS, 216, 29
Brooke, J. S. A., Bernath, P. F., Western, C. M., et al. 2016, JOSRT, 168, 142
Clarke, A. J., Debattista, V. P., Nidever, D. L., et al. 2019, MNRAS, 484, 3476
Demarque, P., Woo, J.-H., Kim, Y.-C., & Yi, S. K. 2004, ApJS, 155, 667
Di Matteo, P. 2016, PASA, 33, e027
Elmegreen, B. G., Bournaud, F., & Elmegreen, D. M. 2008, ApJ, 688, 67
Ernandes, H., Barbuy, B., Friaça, A. C. S., et al. 2020, A&A, 640, A89
Forsberg 2023, PhD thesis, Lund Univ., https://lup.lub.lu.se/search/files/
   160717675/Rebecca_Forsberg_HELA.pdf
Friske, J. K. S., & Schönrich, R. 2023, arXiv:2310.01899
Fulbright, J. P., McWilliam, A., & Rich, R. M. 2007, ApJ, 661, 1152
Gaia Collaboration, Brown, A. G. A., Vallenari, A., et al. 2021, A&A, 650, C3
Gaia Collaboration, Prusti, T., de Bruijne, J. H. J., et al. 2016, A&A, 595, A1
Grevesse, N., Asplund, M., & Sauval, A. J. 2007, SSRv, 130, 105
Grevesse, N., Scott, P., Asplund, M., & Sauval, A. J. 2015, A&A, 573, A27
Grisoni, V., Spitoni, E., Matteucci, F., et al. 2017, MNRAS, 472, 3637
Gully-Santiago, M., Wang, W., Deen, C., & Jaffe, D. 2012, Proc. SPIE, 8450,
Gustafsson, B., Edvardsson, B., Eriksson, K., et al. 2008, A&A, 486, 951
Han, J.-Y., Yuk, I.-S., Ko, K., et al. 2012, Proc. SPIE, 8550, 85501B
Hawkins, K., Masseron, T., Jofré, P., et al. 2016, A&A, 594, A43
```

Hayden, M. R., Bovy, J., Holtzman, J. A., et al. 2015, ApJ, 808, 132

```
Hayes, C. R., Masseron, T., Sobeck, J., et al. 2022, ApJS, 262, 34
Haywood, M., Di Matteo, P., Lehnert, M. D., Katz, D., & Gómez, A. 2013,
     &A. 560, A109
Hill, V., Lecureur, A., Gómez, A., et al. 2011, A&A, 534, A80
Hunter, J. D. 2007, CSE, 9, 90
Immeli, A., Samland, M., Gerhard, O., & Westera, P. 2004, A&A, 413, 547
Jeong, U., Chun, M.-Y., Oh, J. S., et al. 2014, Proc. SPIE, 9154, 91541X
Johnson, C. I., Rich, R. M., Kobayashi, C., Kunder, A., & Koch, A. 2014, AJ,
Johnson, C. I., Rich, R. M., Simion, I. T., et al. 2022, MNRAS, 515, 1469
Jönsson, H., Ryde, N., Nordlander, T., et al. 2017, A&A, 598, A100
Joyce, M., Johnson, C. I., Marchetti, T., et al. 2023, ApJ, 946, 28
Kobayashi, C., Karakas, A. I., & Lugaro, M. 2020, ApJ, 900, 179
Launhardt, R., Zylka, R., & Mezger, P. G. 2002, A&A, 384, 112
Lee, J.-J., Gullikson, K., & Kaplan, K. 2017, Igrins/Plp v2.2.0, Zenodo,
   doi:10.5281/zenodo.845059
Li, G., Gordon, I. E., Rothman, L. S., et al. 2015, ApJS, 216, 15
Lind, K., Amarsi, A. M., Asplund, M., et al. 2017, MNRAS, 468, 4311
Lodders, K. 2003, ApJ, 591, 1220
Lomaeva, M., Jönsson, H., Ryde, N., Schultheis, M., & Thorsbro, B. 2019,
    &A, 625, A141
Manea, C., Hawkins, K., Ness, M. K., et al. 2023, arXiv:2310.15257
Matteucci, F. 2021, A&ARv, 29, 5
Matteucci, F., & Brocato, E. 1990, ApJ, 365, 539
Matteucci, F., Grisoni, V., Spitoni, E., et al. 2019, MNRAS, 487, 5363
McWilliam, A., & Rich, R. M. 1994, ApJS, 91, 749
Meléndez, J., Asplund, M., Alves-Brito, A., et al. 2008, A&A, 484, L21
Montelius, M. 2021, MA thesis, Lund Univ.
Moon, B., Wang, W., Park, C., et al. 2012, Proc. SPIE, 8450, 845048
Nandakumar, G., Ryde, N., Casagrande, L., & Mace, G. 2023a, A&A,
  675. A23
Nandakumar, G., Ryde, N., Forsberg, R., et al. 2024, arXiv:2401.03793
Nandakumar, G., Ryde, N., & Mace, G. 2023b, A&A, 676, A79
Nandakumar, G., Ryde, N., Schultheis, M., et al. 2018, MNRAS, 478, 4374
Ness, M., Freeman, K., Athanassoula, E., et al. 2013, MNRAS, 430, 836
Neumayer, N., Seth, A., & Böker, T. 2020, A&ARv, 28, 4
Nieuwmunster, N., Nandakumar, G., Spitoni, E., et al. 2023, A&A, 671, A94
Nishiyama, S., Yasui, K., Nagata, T., et al. 2013, ApJL, 769, L28
Oh, J. S., Park, C., Cha, S.-M., et al. 2014, Proc. SPIE, 9147, 914739
Park, C., Jaffe, D. T., Yuk, I.-S., et al. 2014, Proc. SPIE, 9147, 91471D
Pignatari, M., Gallino, R., Heil, M., et al. 2010, ApJ, 710, 1557
Portail, M., Wegg, C., Gerhard, O., & Ness, M. 2017, MNRAS, 470, 1233
Prantzos, N., Abia, C., Cristallo, S., Limongi, M., & Chieffi, A. 2020,
   MNRAS, 491, 1832
Queiroz, A. B. A., Anders, F., Chiappini, C., et al. 2020, A&A, 638, A76
Queiroz, A. B. A., Chiappini, C., Perez-Villegas, A., et al. 2021, A&A,
  656, A156
Renaud, F., Agertz, O., Read, J. I., et al. 2021, MNRAS, 503, 5846
Rojas-Arriagada, A., Recio-Blanco, A., de Laverny, P., et al. 2017, A&A,
Rojas-Arriagada, A., Recio-Blanco, A., Hill, V., et al. 2014, A&A, 569, A103
Rojas-Arriagada, A., Zasowski, G., Schultheis, M., et al. 2020, MNRAS,
   499, 1037
Ryde, N., Gustafsson, B., Edvardsson, B., et al. 2010, A&A, 509, A20
Ryde, N., Jönsson, H., Mace, G., et al. 2020, ApJ, 893, 37
Ryde, N., & Schultheis, M. 2015, A&A, 573, A14
Ryde, N., Schultheis, M., Grieco, V., et al. 2016, AJ, 151, 1
Sawczynec, E., Mace, G., Gully-Santiago, M., & Jaffe, D. 2022, AAS Meeting,
   54, 203.06
Schultheis, M., Cunha, K., Zasowski, G., et al. 2015, A&A, 584, A45
Schultheis, M., Rojas-Arriagada, A., Cunha, K., et al. 2020, A&A, 642, A81
Schultheis, M., Rojas-Arriagada, A., Garc'ia Pérez, A. E., et al. 2017, A&A,
   600, A14
Sneden, C., Lucatello, S., Ram, R. S., Brooke, J. S. A., & Bernath, P. 2014,
   ApJS, 214, 26
Spitoni, E., Matteucci, F., Jönsson, H., Ryde, N., & Romano, D. 2018, A&A,
Taylor, M. B. 2005, in ASP Conf. Ser. 347, Astronomical Data Analysis
   Software and Systems XIV, ed. P. Shopbell, M. Britton, & R. Ebert
   (San Francisco, CA: ASP), 29
Thorsbro, B., Forsberg, R., Kordopatis, G., et al. 2023, ApJL, 958, L18
Thorsbro, B., Ryde, N., Rich, R. M., et al. 2020, ApJ, 894, 26
Thorsbro, B., Ryde, N., Schultheis, M., et al. 2018, ApJ, 866, 52
Tody, D. 1993, in ASP Conf. Ser. 52: Astronomical Data Analysis Software
   and Systems II, ed. R. J. Hanisch, R. J. V. Brissenden, & J. Barnes
   (San Francisco, CA: ASP), 173
```

Valenti, J. A., & Piskunov, N. 1996, A&AS, 118, 595
Valenti, J. A., & Piskunov, N., 2012 SME: Spectroscopy Made Easy, Astrophysics Source Code Library, ascl:1202.013
van der Walt, S., Colbert, S. C., & Varoquaux, G. 2011, CSE, 13, 22
Vasiliev, E. 2019, MNRAS, 482, 1525

Virtanen, P., Gommers, R., Oliphant, T. E., et al. 2020, NatMe, 17, 261

SPIE, 7739, 77394L
Wegg, C., & Gerhard, O. 2013, MNRAS, 435, 1874
Yuk, I.-S., Jaffe, D. T., Barnes, S., et al. 2010, Proc. SPIE, 7735, 77351M
Zasowski, G., Schultheis, M., Hasselquist, S., et al. 2019, ApJ, 870, 138
Zoccali, M., Lecureur, A., Barbuy, B., et al. 2006, A&A, 457, L1

Wang, W., Gully-Santiago, M., Deen, C., Mar, D. J., & Jaffe, D. T. 2010, Proc.